Available online at www.sciencedirect.com
SCIENCE DIRECT®
Journal of Nuclear Materials 345 (2005) 245–253
journal of nuclear materials
www.elsevier.com/locate/jnucmat

Synthesis and sintering of $(U_{0.72}Ce_{0.28})O_2$ solid solution

Ashish Jain, K. Ananthasivan, S. Anthonysamy, P.R. Vasudeva Rao *

Fuel Chemistry Division, Chemistry Group, Indira Gandhi Centre for Atomic Research, Kalpakkam 603 102, India

Received 8 March 2005; accepted 9 June 2005

Abstract

Powders of $(U_{0.72}Ce_{0.28})O_2$ solid solution were synthesized through two different procedures, viz., the gel-combustion technique and a modified co-precipitation procedure. These powders were characterized for residual carbon, X-ray crystallite size, specific surface area, microstructure, size distribution of particles and bulk density. Thermal analysis of the precursors revealed that the decomposition behavior of these powders was influenced by the size of their constituent particles. The powder compaction parameters were optimized. Sinterability of the powders was compared using the density of the products obtained by sintering them (1873 K, 4 h) in reducing atmosphere. Most of the powders obtained in this study could be sintered to a density of about 94–96% TD. The morphology of these sintered pellets was studied using SEM. The pellets derived from the powders obtained through the gel-combustion synthesis comprised fine grains and micropores while those obtained from the co-precipitation technique were found to have larger grains and larger pores.

1. Introduction

The conventional methods used in the nuclear industry for fabricating the high-density pellets of the solid solutions of actinide oxides such as $(U,Pu)O_2$, $(U,Th)O_2$ and $(Th,Pu)O_2$ employ powder metallurgical procedures. These techniques involve process steps such as high-energy milling, pre-compaction, granulation, final compaction and sintering at temperatures above 1873 K [1]. When this procedure is adopted meticulous care needs to be taken in order to ensure that the co-milled powder is homogeneous and that the product obtained is a 'single phase' solid solution. In addition to posing problems related to radiotoxicity, these process steps are also energy and cost intensive [2]. Hence, alternate routes that are more energy efficient continue to fascinate the nuclear ceramists. Recent investigations have shown that the gel-combustion synthesis could be an attractive alternative for the synthesis of nuclear ceramics [3]. Ananthasivan et al. [4] reported that conventional precipitation methods could be made to yield more sinteractive powders by de-agglomerating the precursors using ultrasonic waves. Microwave assisted gel combustion is yet another improvisation which is advantageous when the cations like UO_2^{2+} present in the gel are microwave active [5]. Systematic studies are being carried out in our laboratory to develop energy efficient methods for the synthesis of nuclear ceramics such as ThO_2 and $(U,Th)O_2$ [3–5]. As an extension of these studies it was of interest to investigate the gel combustion synthesis of solid solutions of urania and ceria, since cerium is generally known to be a surrogate of plutonium [6,7]. In this study, the gel-combustion synthesis of these

* Corresponding author. Tel.: +91 4114 280098; fax: +91 4114 280065.
E-mail address: vasu@igcar.ernet.in (P.R. Vasudeva Rao).

0022-3115/$ - see front matter © 2005 Elsevier B.V. All rights reserved.
doi:10.1016/j.jnucmat.2005.06.007

powders was investigated. Further, the effectiveness of this method was compared with that of the co-precipitation-de-agglomeration method.

2. Experimental

2.1. Chemicals

Nuclear grade uranium dioxide was obtained from Nuclear Fuel Complex, Hyderabad, India. Cerium(III) nitrate hexahydrade was procured from M/s. Indian Rare Earths Ltd., Mumbai, India. Analytical reagent grade nitric acid was supplied by M/s. Rankem Laboratory Chemicals Pvt. Ltd., Chennai. Liquor ammonia and citric acid were procured from M/s. Fischer Inorganics and Aromatics Ltd., Chennai, India.

2.2. Preparation of the oxide powder by gel combustion synthesis

Uranyl nitrate solution was prepared by dissolving an appropriate quantity of the crystals obtained by reacting U_3O_8 with 12 M nitric acid followed by evaporation of the excess acid. The U_3O_8 used for the above purpose was prepared by oxidizing nuclear grade uranium dioxide powder in air at 1073 K for 4 h with intermediate grinding and homogenization. Cerium nitrate solution was prepared by dissolving cerium(III) nitrate hexahydrate in distilled water.

The combustion mixture was prepared by mixing the above solutions with an appropriate quantity of citric acid. The quantity of citric acid was so chosen that the ratio of citrate ions to that of nitrate ions in the solution was unity. This mixture was heated with intermittent stirring, in a microwave oven (2450 MHz with variable output from 140 to 170 W) supplied by M/s. Batliboi, Mumbai, India. The combustion reaction was taken to completion by heating the charred mass on a hot plate.

2.3. Preparation of the oxide powder by co-precipitation de-agglomeration method

In most of the precipitation experiments, a dense precipitate containing a mixture of ammonium di-uranate and cerium(IV) hydroxide was obtained by the gradual addition of 14 M aqueous ammonia to a mixture of the solutions containing appropriate quantities of uranyl nitrate and cerium(III) nitrate. These experiments are designated as the 'forward strike' experiments. In some experiments, a similar precipitation was carried out by adding the reagents in the reverse order. These experiments are designated as 'reverse-strike'. The powders obtained through the forward strike are designated as 'F' while those obtained through reverse strike are prefixed with 'R'. The dark greenish yellow precipitate obtained in all the above experiments was filtered under suction. One part of the wet precipitate was dispersed in propan-2-one and subjected to ultrasonication in an ultrasonic agitator for 30 min, while the other part was washed with propan-2-one without ultrasonication. The powders subjected to ultrasonication are designated as 'S', while those, which were not de-agglomerated, are called 'WS'. Thus, the designation 'FWS' would represent a powder that was obtained through forward strike and not subjected to ultrasonication. All these powders were dried under an infrared (IR) lamp for half an hour in order to remove the residual moisture present in them.

2.4. Calcination, consolidation and sintering

The combustion product as well as the co-precipitate of precursors were calcined at 1023 K for 5 h in air using a resistance heating furnace fitted with silicon carbide heating elements supplied by M/s. Indian furnaces, Chennai.

The mixed oxide powders obtained in this study were compacted into pellets of two different dimensions viz., (a) with 15 mm diameter and 19 mm length and (b) with 6 mm diameter and 6 mm length. Tools made out of hardened tool-steel were used for the compaction. A double acting hydraulic press supplied by M/s. Bemco Hydraulics Ltd., India, was used for the above purpose. Pre-compaction was carried out at three different pressures, viz., 50, 110, 170 MPa. These pellets were crushed in an agate mortar, and the granules thus obtained were compacted again at a final pressure of about 450 MPa.

The green pellets were sintered at 1873 K for 4 h in a stream of a flowing gas mixture containing 92% argon and 8% hydrogen in a furnace fitted with molybdenum wire heating elements. A typical heating/cooling rate of 5×10^{-2} K s^{-1} was employed.

2.5. Characterization of starting materials, powders and compacts

The impurities present in the starting materials were analyzed using an inductively coupled plasma mass spectrometer (ICPMS), model Elan 250, supplied by M/s. Sciex, Toronto, Canada. The surface area of the powders was measured by the BET method using Monosorb MS-16 surface area analyzer supplied by M/s. Quantachrome Inc., USA. The analysis of the size distribution of particles was carried out using Mastersizer, supplied by M/s. Malvern, Worcestershire, UK. The X-ray powder diffraction patterns were obtained by using XPERT MPD system supplied by M/s. Philips, The Netherlands. The average crystallite size of the powders was measured by X-ray line broadening technique using the Scherrer formula [8]. The instrumental broadening was obtained using standard silicon sample. The density of the green as well as sintered compacts was measured by using

the Archimedes' principle with di-butyl phthalate as the pycnometric liquid. The residual carbon present in the as prepared product, calcined product and the sintered product derived through combustion synthesis was determined by heating the sample in a stream of oxygen and measuring the carbon dioxide generated using an IR detector.

Thermal decomposition of the precursors (FS, FWS, RS and RWS) was studied using TGSDTA851e thermogravimetry – simultaneous differential thermal analyzer (TGSDTA) supplied by M/s. Mettler Toledo, Switzerland. This equipment was calibrated for the temperature measurement using ICTAC recommended standards viz., indium, tin and gold. The thermal decomposition of the precursors, was studied by heating about 10 mg of the powder sample held in an alumina crucible, at a programmed heating rate.

3. Results and discussion

3.1. Purity of the starting materials

The total impurities present in the starting materials used for the preparation of the solid solutions were less than 100 wppm. The metallic impurities like Mg, Ca, V, Nb, Ta and Ti that can affect the sintering process were found to be insignificantly low. Hence, it is reasonable to assume that these impurities did not influence the sinterability of the powders obtained in this study.

3.2. Characteristics of the powders

3.2.1. Bulk density, specific surface area and particle size distribution of the powders

The values of the bulk density as well as the specific surface area of the various powders synthesized in this study are given in Table 1. The size distribution of the particles is given in Table 2 as well as in Fig. 1.

The bulk densities of all the powders obtained by both the methods are comparable. Reduction of the calcined product leads to an increase in its bulk density, which is indicative of better packing. This is probably either due to the introduction of fines in the powder matrix through the disintegration of the bigger particles during reduction or due to the difference in densities of U_3O_8 (8.396 g/cm^3) and UO_2 (10.983 g/cm^3).

The combustion derived powders have a lower surface area compared to those obtained through de-agglomeration. The specific surface area of the precursors derived through both the methods decreases upon calcination in air. This reduction is marginal in the case of the combustion-derived powders while it is quite significant in the case of the powders derived through co-precipitation method. Reduction of these powders brings about only a marginal change in their specific surface area.

It is evident from Fig. 1 that the precursor obtained through co-precipitation comprises fine particles with an average particle size of around 50 μm in a near unimodal distribution. However, the particle size of the precursor obtained through gel-combustion exhibit a bi-modal distribution with peak maxima at 50 and 500 μm.

Table 1
Properties of the $(U_{0.72}Ce_{0.28})O_2$ powder

Powder	Bulk density (mg m^{-3})	Specific surface area (m^{2}g^{-1})	Residual carbon (%)	Crystallite size (nm)
GAP	0.7	5.6	0.65	25
GAC	0.6	4.3	0.01	22
GHC	1.5	5.5	0.01	5
CAP	0.8	35.0	–	7
CAC	1.0	11.0	–	9
CHC	1.1	10.0	–	9

G: gel combustion; **C**: co-precipitated; **AP**: as prepared; **AC**: air calcined; **HC**: calcined in Ar + 8% H_2.

Table 2
Particle size distribution (vol.%) in the solid solutions $(U_{0.72}Ce_{0.28})O_2$

Powder	X vol.% of sample has size less than (μm)		
	$X = 10$	$X = 50$	$X = 90$
GAP	28	418	957
GAC	32	291	995
GHC	43	377	920
CAP	3	25	77
CAC	5	25	72
CHC	2	29	1077

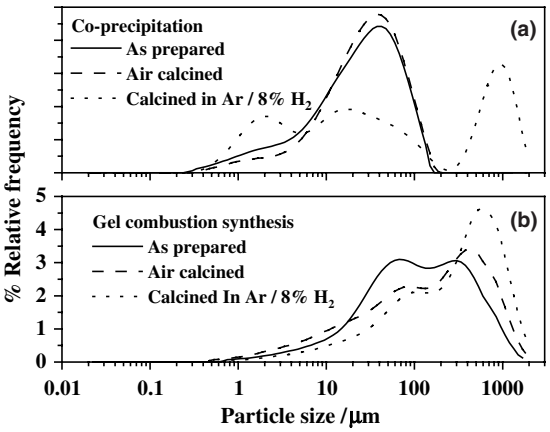

Fig. 1. Particle size distribution of the powder. (a) Powder synthesized by gel combustion method. (b) Powder synthesized by co-precipitation de-agglomeration method.

Calcination of the powders derived through co-precipitation in air does not alter the size distribution. However, the powders derived through gel-combustion show a shift in peak maxima towards higher values upon reduction. Calcination in hydrogen brings about a trimodal distribution with peak maxima at 1, 10 and 500 μm in the powder derived through co-precipitation. The size of the particles in the powders derived through gel-combustion marginally increases upon calcination in hydrogen. These trends in the bulk density, specific surface area and the particle size distribution could be explained as follows.

During calcination in both air as well as in hydrogen the constituent particles in the powders derived through the gel-combustion method progressively grow due to pre-sintering. It is also expected that fines would be introduced into the matrix during hydrogen calcination, due to crumbling of the particles brought about by the shrinkage of the hyper stoichiometric (oxygen to metal ratio, $O/M > 2$) oxide into a less voluminous stoichiometric oxide ($O/M = 2$). However, the observed 'net increase' in the particle size in the calcined product is probably due to the dominant role played by the pre-sintering.

The powders derived through co-precipitation undergo decomposition during calcination with an attendant decrease in specific surface area. Under the oxidizing conditions prevalent during calcination, particle growth is predominant, which compensates the reduction in size due to decomposition. Hence, on the whole no observable variation in the size distribution is observed. However, during the hydrogen reduction these particles disintegrate, yielding a greater fraction of fines. The particle growth during the hydrogen calcination leads to the production of a definite fraction of bigger particles as well. The difference in the variation of size distribution in these two powders stems from the fact that the combustion product contains predominantly a homogeneous solid solution while the powder derived through co-precipitation is biphasic.

3.2.2. X-ray crystallite size of the powder

The X-ray diffraction pattern of the powders at different stages of synthesis is shown in Figs. 2 and 3. It is evident from the XRD of the combustion derived product that it comprises the solid solution, U_3O_8, CeO_2 and traces of UO_3. On the other hand, the powder obtained through the co-precipitation method is a homogenous mixture of the two oxides viz., U_3O_8 and CeO_2. This mixture yields the solid solution only after sintering at a high temperature.

All the powders synthesized in this study were found to be nano-crystalline. The crystallite sizes of the combustion-derived powders are in the range of 20–25 nm. The crystallite sizes of the de-agglomerated powders are less than 10 nm in all the three stages. No substantial change was observed in the crystallite sizes of the co-precipitated powders when the calcination atmosphere was changed from air to $Ar + H_2$. This indicates that ultrasonication of the precursor in non-aqueous media helps in producing nanocrystalline particles and the crystallite size of the product derived from them is not affected significantly by the variations in the calcination conditions. On the other hand, the crystallite size of the powders derived from combustion synthesis reduces to 5 nm when the calcination is carried out in a reducing atmosphere.

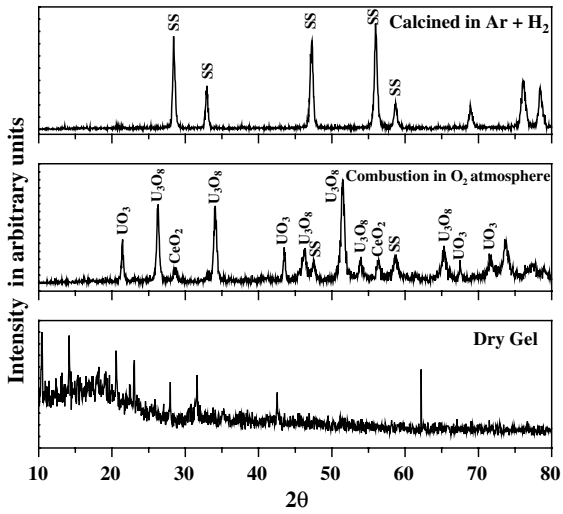

Fig. 2. XRD pattern of the powders synthesized in this study (gel combustion).

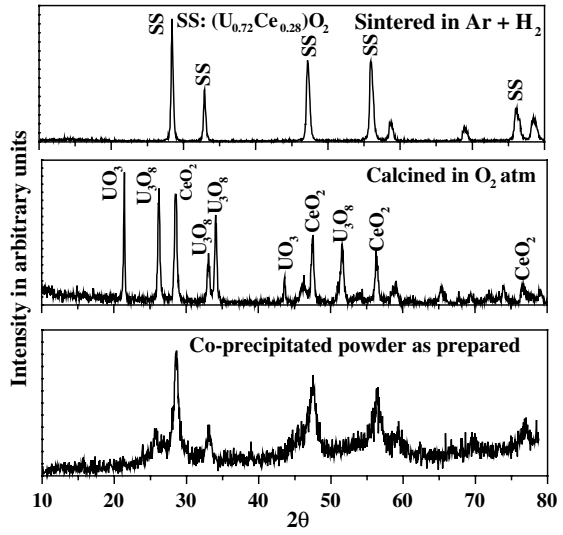

Fig. 3. XRD pattern of the powders synthesized in this study (co-precipitation).

3.2.3. Residual carbon in the powder

The residual carbon present in the powder derived through combustion synthesis is given in Table 1. Previous studies have shown that the residual carbon content depends on the calcination temperature and duration of the calcination [9]. It is also influenced by the nature of the fuel material (the carbon chain length of the fuel) used for the synthesis. The results of the carbon analysis show that the residual carbon content in the as-prepared powder is high. This is due to the incomplete burning of the fuel at the temperature prevailing during the combustion synthesis. The residual carbon content of the combustion derived powder after air calcination and after calcination in reducing atmosphere are almost the same. This shows that the carbon left after the combustion step had undergone complete oxidation during calcination in air.

The precursors derived from the co-precipitation method do not have any carbonaceous residue. Since the carbon residue in the starting material was insignificantly low, no attempt was made to determine the carbon content in the powder derived through the co-precipitation method.

3.2.4. Thermal studies on the gel combustion synthesis

The thermograms pertaining to the decomposition of the metal nitrates, citric acid as well as the gel are given in Fig. 4(a) and (b). The thermograms pertaining to the decomposition of the nitrates are similar to those reported in an earlier study [10]. The thermograms pertaining to the decomposition of the gel are shown in Fig. 5. These thermograms suggest that there are two distinct steps are involved in the gel-combustion reaction, viz., loss of water (373–393 K) and the combustion reaction. The gel gets completely dried at around 423 K leaving behind a yellow porous mass. Upon further heating, the nitrates of uranium and cerium are decomposed with an attendant oxidation of citric acid. This leaves behind an oxide residue that contains significant amounts of carbon. Subsequently, the residual carbon gets oxidized in a slow and continuous manner. From Fig. 5 it is apparent that the self-sustaining and exothermic combustion reaction sets in at around 573 K. The X-ray diffractogram of this product revealed that it contained a substantial quantity of U_3O_8. The very high oxygen potential that prevailed during this experiment was responsible for the precipitation of U_3O_8 from the mixed oxide matrix. When the same powder was calcined in $Ar + 8\%$ H_2, weight loss was observed at 873 K as shown in Fig. 4(c), which could be ascribed to the reduction of U_3O_8 to UO_2.

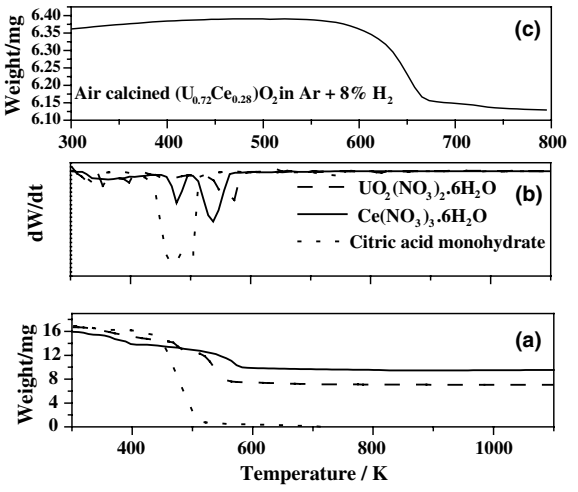

Fig. 4. (a) Thermograms pertaining to the decomposition of uranyl nitrate, cerium(III) nitrate hexahydrate and citric acid. (b) Derivative thermograms pertaining to the decomposition of uranyl nitrate, cerium (III) nitrate hexahydrate and citric acid. (c) Thermogram pertaining to the loss of weight in a hyper stoichiometric product (O/M > 2).

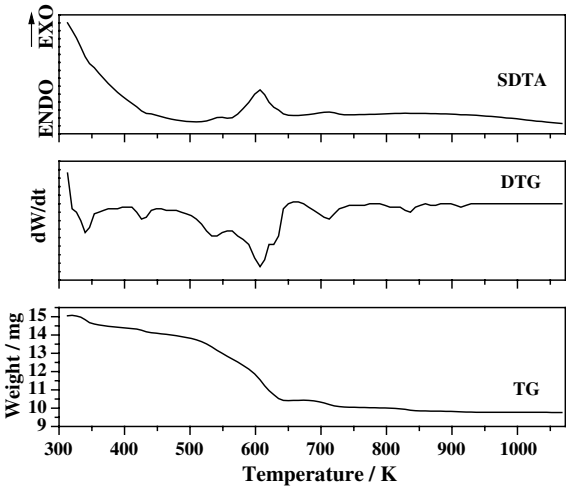

Fig. 5. Thermal analysis of the citric acid gel combustion reaction involving uranyl nitrate and cerium(IV) nitrate.

3.2.5. Thermal studies on the co-precipitated precursors

Thermograms (DTG) pertaining to the decomposition of a co-precipitate of ceric hydroxide and ammonium diuranate are shown in Fig. 6. Thermograms pertaining to the decomposition of cerium(IV) hydroxide and ADU are also shown in the same figure. From these thermograms it is apparent that $Ce(OH)_4$ decomposes in two steps. The first weight loss starting at 303 K is due to the loss of moisture present in the precipitate. The second weight loss occurring at around 600 K could be attributed to the conversion of cerium(IV) hydroxide to cerium (IV) oxide involving multiple steps. ADU begins to lose moisture at around 303 K. Conversion of the dry ADU to the oxides of uranium takes

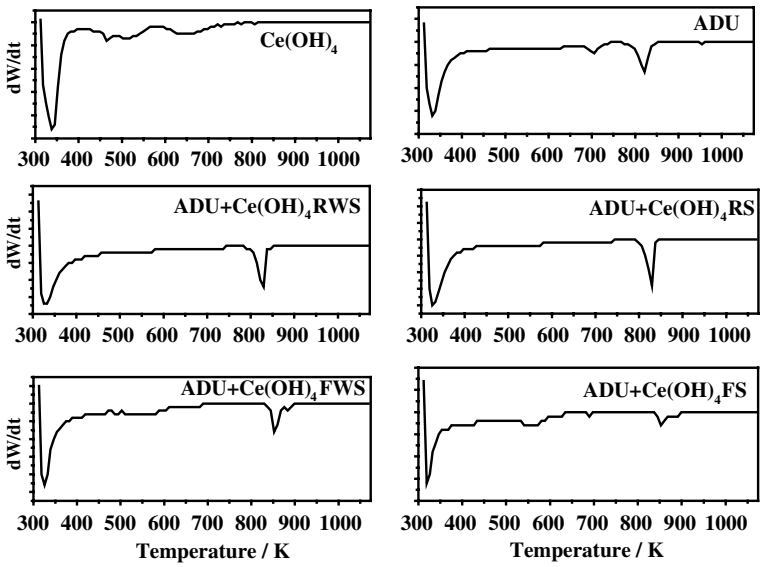

Fig. 6. DTG curves pertaining to the thermal decomposition of ammonium di-uranate and cerium(IV) hydroxide.

place between 650 and 900 K. This decomposition also involves multiple steps. The thermogram of the co-precipitated precursor shows two weight loss steps. The first one at 303 K corresponds to the loss of water present in the powder. The second occurring beyond 800 K corresponds to the decomposition of the homogenous mixed precursors.

Oktay and Yayli [11] carried out DTA measurements on thorium oxalate powders prepared through different routes. They reported that the decomposition process occurs over a temperature range. This temperature range reduces when thorium oxalate is ultra-sonicated in a non-aqueous media. However, such a trend was not observed in the thermograms of the co-precipitates investigated in the present study. Nevertheless, the order of addition of the reagents is seen to affect the span of these DTA plots. The decomposition of those precursors that were prepared by the reverse strike takes place over a wider range of temperature. The reverse addition of the reagents also brings down the onset as well as the terminal temperatures of the decomposition as shown in Table 3. This shows that the reverse addition of the reagents can reduce the duration of calcination and help in completing calcination at a relatively lower temperature. These effects could be ascribed to the presence of a higher fraction of fine powders in the samples obtained through the reverse strike procedure.

Table 3
On set and termination temperatures in the decomposition of the hydroxide precipitates

Hydroxide precursor of $(U_{0.72}Ce_{0.28})O_2$	Onset temperature	End set temperature
FS	840.4	860.8
FWS	845.4	861.9
RS	808.7	832.3
RWS	812.3	832.5

3.3. Characteristics of the green and sintered pellets

3.3.1. Consolidation of the powders and sintering

Attempts were made to consolidate the powders into pellets having two different dimensions without the addition of a binder. It was found that the green pellets had defects such as end-capping and chipping. In order to prepare defect free green pellets, 0.3 wt% of zinc behenate was added as a binder. During sintering, these pellets were soaked at 673 K for one hour in order to remove the binder completely.

3.3.2. Morphology of the powder and microstructure of the sintered pellets

The morphology of the powders derived using co-precipitation de-agglomeration method and combustion synthesis are shown in Figs. 7 and 8 respectively. The co-precipitated powder is composed of irregular particles of different sizes. The powders derived through combustion synthesis exhibit fractured surfaces and show a high

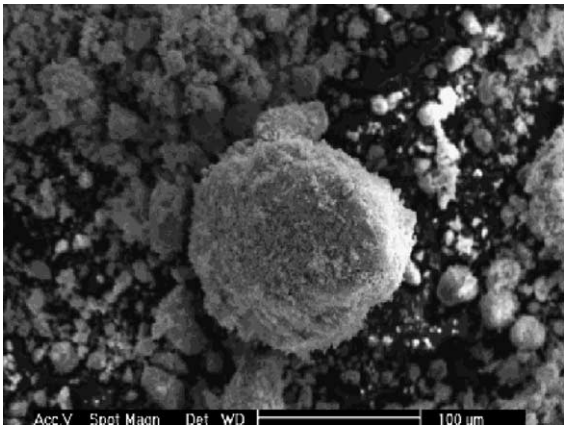

Fig. 7. SEM of the powder derived by co-precipitation method.

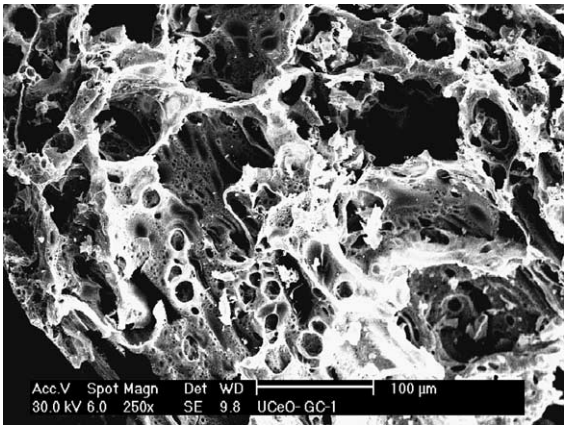

Fig. 8. SEM of the powder derived by combustion synthesis.

degree of porosity. The presence of porosity is a common feature observed in the powders derived through gel-combustion [9]. These are probably introduced into the precursor matrix during the combustion reaction.

The SEM images of the sintered pellets are shown in the Figs. 9–11. The image shown in Fig. 9 is for the pellet consolidated using co-precipitation derived powder, which shows a high degree of closed porosity. The SEM image of the sintered pellet derived through combustion synthesis is shown in Fig. 10. This pellet has less porosity. The SEM image of the surface obtained after slicing the pellet vertically shows the presence of open porosity at some places. In general it could be concluded that pore elimination had taken place during sintering to a significant extent.

3.3.3. Variation of green and sintered densities with compaction pressure

Owing to their low bulk densities the powders prepared in this study had to be pre-compacted and granu-

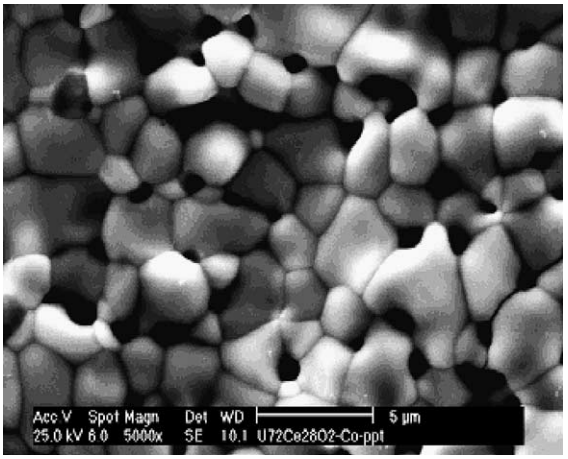

Fig. 9. SEM image of the sintered pellet prepared by the powder derived form the co-precipitation-de-agglomeration method.

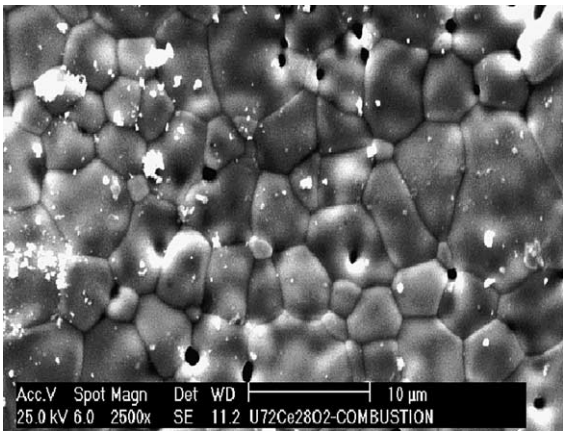

Fig. 10. SEM image of the sintered pellet prepared from the powder derived form the combustion synthesis.

lated prior to final compaction. In order to arrive at the right compaction parameters we studied the effect of the pre-compaction pressure on the physical characteristics of the pellet as well as the final density. The green densities of over 20 pellets prepared in an individual trial were analyzed and the mean of these values is present in the Tables 4 and 5. In general, it is expected that the combustion-derived powders would get compacted to higher densities at lower pressures, owing to the poor strength of the agglomerates present in them [12]. From the results obtained in this study it appears that a pre-compaction pressure of around 170 MPa is good enough to slug all the powders obtained in this study.

Commercial processes employed in the fabrication of nuclear grade uranium oxide pellets aim at achieving a typical green density in the range of 55–60% TD.

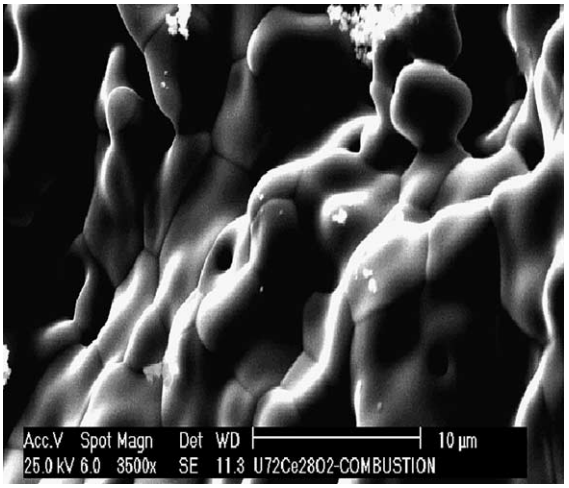

Fig. 11. SEM image of a vertical slice of a sintered pellet prepared from the powder derived from combustion synthesis.

However, we could not consolidate the powders obtained in this study into 'defect free' greens with such a density. A higher die wall friction created by the fines resulted in end capping and lamination of the green compacts, when a pressure in excess of 500 MPa was employed for consolidation. These pellets were made using the +300 μm fraction of the pre slugged granules. Probably, the facile fragmentation of these granules resulting in a higher fraction of finer particles at higher pressures was responsible for the die wall friction. Hence, the compaction pressures were to be limited to 450 MPa. When one specific lot of a powder obtained through co-precipitation route was compacted with a final compaction pressure of 170 MPa a green density of about 51.5% TD could be obtained. However, these pellets sintered with an extensive hour-glassing and a density of only about 92% TD. Hence, it appears that even though a compaction pressure of about 170 MPa is sufficient to facilitate fracture, the density profiles in the green compact are quite inhomogeneous. In general, the gel-combustion derived powders yielded a final product with a higher density compared to the powders derived through co-precipitation. It was observed in an earlier study on thoria [12] that the low agglomerate strength and nanoporosity make the gel combustion derived product more sinterable compared to the powder derived through precipitation. This explains the higher sinterability of the gel-combustion derived powders observed in this study as well.

Table 4
Density of the compacts (diameter: 14 mm, height: 18 mm)

S. no.	Pre-compaction (MPa)	Final compaction (MPa)	Green density (% TD)	Sintered density (% TD)	Heating rate (K min^{-1})
Co-precipitation de-agglomeration					
1	50	340	46.4	94.0	12
2	110	340	49.6	94.4	12
3	170	170	51.5	91.6	12
4	170	450	50.1	96.2	3
Combustion synthesis					
1	50	340	46.7	94.2	12
2	110	340	47.2	95.1	12
3	170	450	48.9	96.1	3
4	170	450	49.1	96.5	3
5	170	450	51.5	96.8	3

Table 5
Density of the compacts (diameter: 6 mm, height: 6 mm)

Pre-compaction (MPa)	Final compaction (MPa)	Green density (% TD)	Sintered density (% TD)	Heating rate (K min^{-1})
Co-precipitation de-agglomeration				
150	250	48.3	88.1	12
170	350	50.2	89.6	3
180	450	53.5	94.2	3
Combustion synthesis				
150	250	48.3	91.5	12
170	350	50.5	94.3	3
180	450	52.1	96.2	3

All the powders obtained in this study yielded a final product with a higher density when the pellet diameter was larger. This could be attributed to the experimental artifacts arising from improper compaction. Even though enough care was taken to minimize the die wall friction by providing an 'ejection taper' of about 0.3 mm over the height of the compact in order to facilitate gradual stress release during its spring back, these could not be suppressed. Probably, the use of a tooling made out of a harder material viz. tungsten carbide would eliminate these differences.

The value of 450 MPa is marginally more than the critical compaction pressure required for obtaining a green density of about 55–60% TD for UO_2 cited by Balakrishna et al. [13]. The critical compaction pressures for powders of ceria derived through the conventional powder metallurgical procedure as well as the gel-combustion route are not available. In the absence of these values it is not possible to compare the strength the agglomerates used in the present study with those pertaining to ceria-urania derived through conventional methods.

Further it was observed that the rate at which these samples are heated during the sintering cycle has a bearing on the sintered density. The desired sintered densities >95% of TD could not be achieved for co-precipitated derived powders when a heating rate of 12 K min^{-1} was employed to reach sintering temperature. However, the highest sintered density of about 96.8% TD was obtained for combustion derived powders by employing a heating rate of 3 K min^{-1}. A similar trend is observed for the pellets with smaller diameter as well as given in Table 5.

4. Conclusions

The present study leads to the following conclusions:

1. High density (96% TD) pellets of urania-ceria solid solution of composition $(U_{0.72}Ce_{0.28})O_2$ could be prepared using the gel-combustion synthesis as well as the co-precipitation method.
2. The decomposition of the gel containing uranyl nitrate, cerium nitrate and citric acid is completed at 773 K. The combustion product is a mixture of the solid solution and oxides of uranium and cerium.
3. The co-precipitation route yields an intimate physical mixture of the two oxides that could be converted into a solid solution by heating at higher temperatures.
4. In order to adjust the oxygen stoichiometry, it is essential to calcine all the products obtained in a reducing atmosphere (Ar + 8% H_2).
5. The powders derived from the gel combustion synthesis show better sinterability than the powers derived form the modified co-precipitation route.

References

[1] H. Assmann, H. Bairiot, Process and product control of oxide powder and pellets for reactor fuel application, in: Guide book on Quality Control of Water Reactor Fuel, Tech. Report Series No. 221, IAEA, Vienna, 1983, p. 149.
[2] J.M. Pope, K.C. Radford, J. Nucl. Mater. 52 (1974) 241.
[3] V. Chandramouli, S. Anthonysamy, P.R. Vasudeva Rao, R. Divakar, D. Sundararaman, J. Nucl. Mater. 231 (1996) 213.
[4] K. Ananthasivan, S. Anthonysamy, A. Singh, P.R. Vasudeva Rao, J. Nucl. Mater. 306 (2002) 1.
[5] S. Anthonysamy, K. Ananthasivan, V. Chandramouli, P.R. Vasudeva Rao, J. Nucl. Mater. 278 (2000) 346.
[6] D.G. Kolman, Y. Park, M. Stan, R.J. Hanrahan Jr., D.P. Butt, Los Alamos National Laboratory Report, LA-UR-99-491, 1999.
[7] W. Dorr, S. Hellmann, G. Mages, J. Nucl. Mater. 140 (1986) 7.
[8] H.P. King, L.E. Alexander, X-ray Diffraction Procedures for Polycrystalline and Amorphous Materials, Wiley, USA, 1954.
[9] S. Anthonysamy, PhD Thesis, University of Madras, Chennai, India, 2000.
[10] S. Dash, M. Kamruddin, S. Bera, P.K. Ajikumar, A.K. Tyagi, S.V. Narasimhan, B. Raj, J. Nucl. Mater. 264 (1999) 271.
[11] E. Oktay, A. Yayli, J. Nucl. Mater. 288 (2001) 76.
[12] K. Ananthasivan, PhD Thesis, University of Madras, Chennai, India, 2003.
[13] P. Balakrishna, B.P. Varma, T.S. Krishnan, T.R.R. Mohan, P. Ramakrishnan, J. Nucl. Mater. 160 (1988) 88.